Molecules and Cells

The Crystal Structure of L-Leucine Dehydrogenase from *Pseudomonas aeruginosa*

Seheon Kim[1], Seri Koh[1], Wonchull Kang[1,2,*], and Jin Kuk Yang[1,*]

[1]Department of Chemistry, College of Natural Sciences, Soongsil University, Seoul 06978, Korea, [2]Department of Physics and Integrative Institute of Basic Science, Soongsil University, Seoul 06978, Korea
*Correspondence: jinkukyang@ssu.ac.kr (JKY); wonchullkang@ssu.ac.kr (WK)
https://doi.org/10.14348/molcells.2022.0012
www.molcells.org

Leucine dehydrogenase (LDH, EC 1.4.1.9) catalyzes the reversible deamination of branched-chain L-amino acids to their corresponding keto acids using NAD^+ as a cofactor. LDH generally adopts an octameric structure with *D4* symmetry, generating a molecular mass of approximately 400 kDa. Here, the crystal structure of the LDH from *Pseudomonas aeruginosa* (*Pa*-LDH) was determined at 2.5 Å resolution. Interestingly, the crystal structure shows that the enzyme exists as a dimer with *C2* symmetry in a crystal lattice. The dimeric structure was also observed in solution using multiangle light scattering coupled with size-exclusion chromatography. The enzyme assay revealed that the specific activity was maximal at 60°C and pH 8.5. The kinetic parameters for three different amino acid and the cofactor (NAD^+) were determined. The crystal structure represents that the subunit has more compact structure than homologs' structure. In addition, the crystal structure along with sequence alignments indicates a set of non-conserved arginine residues which are important in stability. Subsequent mutation analysis for those residues revealed that the enzyme activity reduced to one third of the wild type. These results provide structural and biochemical insights for its future studies on its application for industrial purposes.

Keywords: branched-chain amino acid, leucine dehydrogenase, PA3418, *Pseudomonas aeruginosa*

INTRODUCTION

Leucine dehydrogenase (LDH, EC 1.4.1.9) catalyzes the reversible deamination of L-leucine and other branched-chain L-amino acids (BCAAs) to their corresponding keto derivatives using NAD^+ as a cofactor (Fig. 1). LDH belongs to the Glu/Leu/Phe/Val dehydrogenase family. The enzymes of this family are considered important for incorporating ammonia into organic compounds and are the link between metabolism of carbohydrates and that of amino acids (Turnbull et al., 1994).

LDH has been characterized in many Bacillus species, where it metabolizes the catabolism of branched-chain amino acids (Ohshima et al., 1978; 1985). This enzyme is also useful for quantifying of BCAAs such as leucine, isoleucine, and valine in the clinical field (Beckett et al., 1996; Suzuki et al., 2008). Patients with hepatitis C virus (HCV)-associated chronic liver diseases have a low amount of BCAAs in their

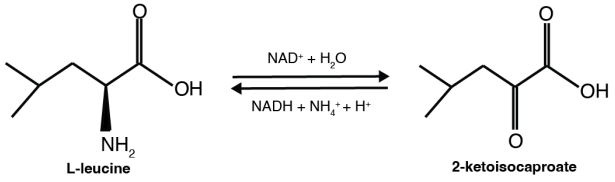

Fig. 1. Reaction catalyzed by the LDH.

Received 29 October, 2021; revised 4 February, 2022; accepted 24 February, 2022; published online 14 June, 2022

eISSN: 0219-1032

blood, which causes a reduction in the BCAAs/tyrosine molar ratio and the Fisher ratio (molar ratio between BCAAs and aromatic amino acids) (Tajiri and Shimizu, 2013). Thus, the concentration of BCAAs is a good indicator of this disease (Suzuki et al., 2008). Furthermore, LDH can be used for the stereoselective production of BCAAs (Gu and Chang, 1990a; 1990b). Chiral amines and L-tert-leucine are selectively synthesized by variants of LDH (Abrahamson et al., 2012; Meng et al., 2021). The atomic structure of an enzyme is critical for protein engineering in a wide range of fields.

The quaternary structure of LDH has been reported as an octamer with *D4* symmetry, whose subunit has two distinct domains (Baker et al., 1995; Turnbull et al., 1994; Yamaguchi et al., 2019; Zhao et al., 2012). The first domain is a core domain associated with the adjacent subunit, and the other is known as the nucleotide-binding domain with a Rossman fold. A deep groove at the junction of the two domains was assumed to be a substrate-binding site. Recently, single-particle cryo-electron microscopic studies of LDH from *Geobacillus stearothermophilus*, a thermophile, revealed the structure of the apo- and NAD^+-bound form at 3.0 Å and 3.2 Å resolution, respectively (Yamaguchi et al., 2019). Comparing the two conformations showed that NAD^+ binding induced conformational changes at the oligomeric interface and that some residues at the interface are important for thermostability and activity (Yamaguchi et al., 2019). It has been clarified that most of the reported structures adopt an open conformation that allows the binding of NAD^+ close to the native conformation in solution (Yamaguchi et al., 2019). However, the activity of enzymes from thermophiles, particularly hyperthermophiles, is slowly reduced with a reduction in temperature. Thus, enzymes from thermophiles are not always practical for use at low temperatures.

To gain a better understanding of LDH from *Pseudomonas aeruginosa* (*Pa*-LDH) at a molecular and biochemical level, we performed a structural and biochemical characterization in this study. The enzyme parameters were determined by an *in vitro* enzyme assay. The crystal structure determined at 2.5 Å resolution reveals that the quaternary structure is a dimer with *C2* symmetry in the crystal lattice. The dimer has also been observed in solution using multiangle light scattering (MALS) coupled with size-exclusion chromatography (SEC). In addition, the structural and biochemical studies imply that non-conserved three arginine residues contribute to the stability. Our key findings are to show the atomic detail how *Pa*-LDH gains stability by the changed of tertiary and quaternary structures.

MATERIALS AND METHODS

Cloning, expression, and purification

The LDH amplified from *P. aeruginosa* genomic DNA (ATCC 15692, USA) was cloned into a modified pET-26b vector at the NdeI and BamHI restriction sites. Nucleotide sequences were confirmed by sequencing (Bionics, Korea). The LDH-His_6 protein was expressed in *Escherichia coli* strain Rosetta 2 (DE3). A single colony was inoculated in 10 ml Luria-Bertani (LB) medium supplemented with kanamycin (50 mg ml^{-1}) to grow an overnight culture at 310 K. This culture was diluted in 1 L of LB medium supplemented with kanamycin (50 mg ml^{-1}). The cells were grown at 310 K to an OD_{600} of 0.6, the culture was cooled to 298 K, and protein expression was induced by adding isopropyl β-D-thiogalactopyranoside (IPTG) to a final concentration of 0.5 mM. The cells were grown overnight at 298 K. The cells were harvested via centrifugation at 2,780 × *g* for 20 min (Supra 22 K with rotor 11; Hanil Scientific, Korea) and resuspended in a working buffer (20 mM Tris-HCl, 5% (v/v) glycerol, 0.1 mM TCEP, 100 mM sodium chloride) supplemented with 0.1 mM phenylmethylsulfonyl fluoride, and 10 mM imidazole. The cells were disrupted via sonication and cell debris were removed via centrifugation at 24,650 × *g* for 60 min (Supra 22 K with rotor 7; Hanil Scientific). The supernatant was filtered through a membrane filter with 0.45-mm pore size membrane filter (Millipore, USA) and loaded onto a HisTrap FF column (Cytiva, USA). The bound protein was eluted with a 0-0.5 M imidazole gradient. The pooled sample was further purified using SEC (HiLoad 16/600 Supderdex200; Cytiva). The final purified sample was concentrated to 9 mg ml^{-1} via centrifugal ultrafiltration (Amicon Ultra; Millipore, USA). The purity of the isolated protein was estimated through SDS-PAGE, and the concentration was determined by measuring the absorbance at 280 nm using a calculated extinction coefficient of 4.18 mg^{-1} ml cm^{-1} (Gasteiger et al., 2005). The final buffer contains 20 mM Tris-HCl, 5% (v/v) glycerol, 0.1 mM TCEP, and 100 mM sodium chloride at pH 8.0.

Crystallization and X-ray data collection

Initial crystallization screening was performed in sitting drops by mixing 1.0 ml protein solution with 1.0 ml reservoir solution of commercial screening kits such as SaltRx, Index, and PEG/ION screens (Hampton Research, USA) on 96-well Swissci MRC plates (SWISSCI, Switzerland) at 295 K. Several hits were obtained, and crystal optimization was performed by varying the concentration of the components. The final optimized composition was 12% (w/v) polyethylene glycol (PEG) 3350 and 0.1 M sodium acetate trihydrate. The size of the crystals reached the maximum dimensions after a month, with typical dimensions of 0.1 mm × 0.1 mm × 0.3 mm. For cryoprotection, the concentrations of glycerol and PEG 3350 were continuously increased to 20% (w/v) PEG 3350 and 20% (v/v) glycerol. The crystal was taken from the drop and directly flash-frozen in liquid nitrogen before data collection. Data were collected at the 11C beamline of the Pohang Accelerator Laboratory (Korea) using a PILATUS 3 6M detector (DECTRIS, Switzerland) at a wavelength of 0.9794 Å and a crystal-to-detector distance of 400.0 mm. A total of 360 images were collected with an exposure time of 1 s and 1° oscillation. The data-collection statistics are listed in Supplementary Table S1.

Structure solution and refinement

Intensity of the data were processed, merged, and scaled using *MOSFLM* and *SCALA* from the *CCP4* program suite (Winn et al., 2011). The initial model of the crystal structure was determined via molecular replacement using MrBump in the CCP4 program suite (Winn et al., 2011). The model was iteratively refined using phenix.refine in the PHENIX suite (Liebschner et al., 2019) and manually rebuilt using Coot (Abra-

hamson et al., 2012; Emsley et al., 2010). Water and glycerol were added and inspected manually using Coot and further refined using phenix.refine in the PHENIX suite (Liebschner et al., 2019). The refinement statistics are presented in Supplementary Table S1. The coordinates and structure factors were deposited in the worldwide Protein Data Bank (PDB entry: 7VID). The X-ray diffraction data are available on the website (https://www.proteindiffraction.org/).

SEC combined with MALS

SEC-MALS was performed on an HPLC system (Shimadzu, Japan) connected to a DAWN HELEOS II system with an Optilab rEX refractive index (RI) detector (Wyatt Technology, USA). A Superdex-200 Increase HR 10/300 GL column (Cytiva) was used with a buffer containing 20 mM Tris-HCl (pH 8.0), 0.1 mM TCEP, 100 mM NaCl, and 5% (v/v) glycerol at a flow rate of 0.5 ml min-1. ASTRA software (ver.6.0) was used to acquire and analyze UV, RI, and MALS data.

Thermal denaturation using circular dichroism (CD) spectroscopy

CD measurements were conducted in a Jasco J-1500 spectropolarimeter (Jasco, UK) at a wavelength of 222 nm as a function of temperature. The protein was heated at the temperature range of 25°C to 95°C at a heating rate of 1°C min^{-1}, equilibrated for at least 2 min at each temperature, and the CD data were collected at 5-s intervals. Three independent measurements were averaged, after eliminating the CD signals from the buffer.

Enzyme assay

LDH enzyme activity was determined by measuring the increase in absorbance at 340 nm for the NADH produced in the reaction. The reaction was initiated by adding the limiting amount (117 ng in 0.4 μl) of the enzyme to the reaction mixture and was monitored at 340 nm using an Ultrospec 8000 UV-Visible spectrophotometer (Cytiva). Three independent measurements were obtained.

RESULTS AND DISCUSSION

The overall structure of LDH from *P. aeruginosa*

The crystal structure of *Pa*-LDH was determined at a resolution of 2.5 Å and refined to 19.6% for R_{work} and 24.9% for R_{free}. The refinement statistics are presented in Supplementary Table S1. There are two subunits in the asymmetric unit with *C2* symmetry as noncrystallographic symmetry (Fig. 2). According to the validation report from the PHENIX suite, 98.37% of the residues were in the favored region of the Ramachandran plot.

A sequence alignment of *Pa*-LDH with other homologs from *Lysinibacillus sphaericus* (*Lsp*-LDH), *G. stearothermo-*

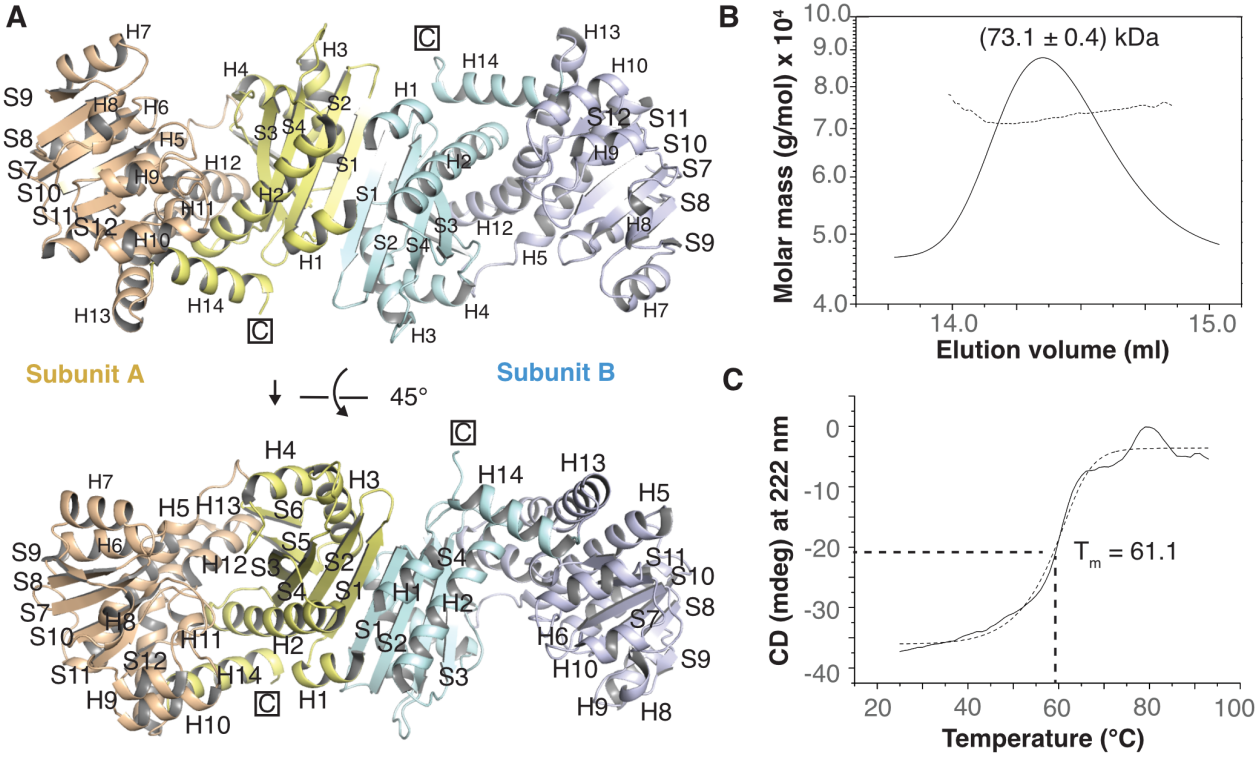

Fig. 2. Overall *Pa*-LDH fold and its dimeric assembly. (A) Representations of the crystal structure of *Pa*-LDH at a 2.5 Å resolution (PDB entry: 7VID) illustrating a dimeric assembly with individual chains colored as follows: domain I of subunit A, yellow; domain II of subunit A, orange; domain I of subunit B, cyan; domain II of subunit B, light purple. (B) The SEC-MALS profile exhibits a distinct single peak that represents the molecular mass of the dimeric assembly. (C) Thermal denaturation curve monitored via CD spectroscopy at a wavelength of 222 nm.

philus (*Gst*-LDH), and *Sporosarcina psychrophiles* (*Sps*-LDH), is shown in Supplementary Fig. S1. Their sequence identities were 48%, 47%, and 46% to *Pa*-LDH. *Pa*-LDH does not have a tail at the C-terminus that contributes to the assembly of the quaternary structure (Yamaguchi et al., 2019; 2021).

The crystal structure of the *Pa*-LDH consists of 14 α-helices and 12 β-strands, and a deep cleft separates the two domains. Domain I is the core domain consisting of residues 1-133 and 324-341, and is related to dimer formation, while domain II, known as the nucleotide-binding domain (residues 134-323), has a six-stranded parallel β-sheet (β9↑ – β8↑ – β7↑ – β10↑ – β11↑ – β12↑) flanked by six α-helices, including a feature of a dinucleotide-binding motif (Supplementary Fig. S2).

Interestingly, the quaternary structure of *Pa*-LDH is a dimer in the crystal lattice, as well as in solution, as confirmed using SEC-MALS (Figs. 2A and 2B). An octamer was not observed in the crystal lattice when symmetry mates were generated using a crystallographic operation (Supplementary Fig. S3). Although *Pa*-LDH exists as a dimer, it has similar thermostability (T_m = 61.1°C) with *Lsp*-LDH, a octameric enzyme from a mesophile, which is stable up to 60°C (Ohshima et al., 1978) (Fig. 2C). Since both enzymes are derived from mesophiles, the same thermostability can be inferred from the comparison of the crystal structures. The thermostability of *Pa*-LDH is mainly come from the dimeric structure, while the *Lsp*-LDH is stabilized by the octameric assembly. Notably, we found the unique two features of *Pa*-LDH which were contributed to the thermostability. The features including the atomic detail were described in the following sections.

Intermolecular interactions between adjacent subunits

Our crystal structure is shown a dimeric LDH with *C2* symmetry, while other homologs exist as an octamer with *D4* symmetry. A tail at the C-terminus is contributed to the interactions made between the four dimers around the fourfold axis in *Lsp*-, *Gst*-, and *Sps*-LDH (Baker et al., 1995; Turnbull et al., 1994; Yamaguchi et al., 2019; Zhao et al., 2012). As *Pa*-LDH is a relatively short isoform lacking a tail at the C-terminus, *Pa*-LDH cannot extend beyond the dimeric structure. The dimeric interface is reminiscent of the homolog. The main interactions between two subunits are come from residues in domain I which interact with each other across the two-fold axis (Fig. 3). The β-strand (S1) from subunit A interacts with the other β-strand (S1) from subunit B in an antiparallel manner to form a sheet of 12 strands. In addition, an amide group of Phe2 forms a hydrogen bond with a carboxyl group of Asp-49 from the other subunit, and an amide group and a carbonyl oxygen of Ser-103 form hydrogen bonds with a carbonyl oxygen and an amide group of Arg-107, respectively. The side chain of Ser-103 also forms a hydrogen bond with the side chain of Arg-107.

Intramolecular interactions in the subunit

The subunit of *Pa*-LDH was aligned with *Lsp*-LDH (PDB ID:

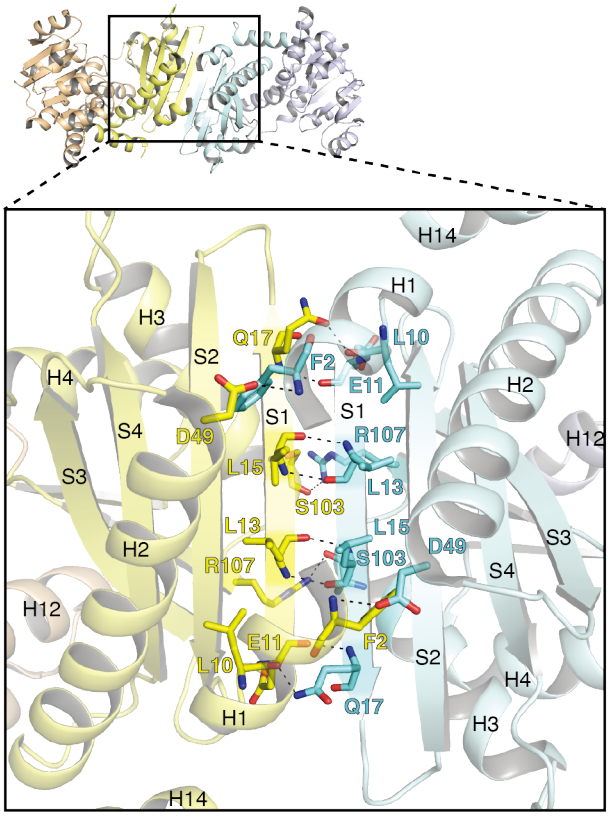

Fig. 3. A dimeric structure of *Pa*-LDH. The atomic details of the dimer interface are shown in stick models. The dashed line represents the H-bond.

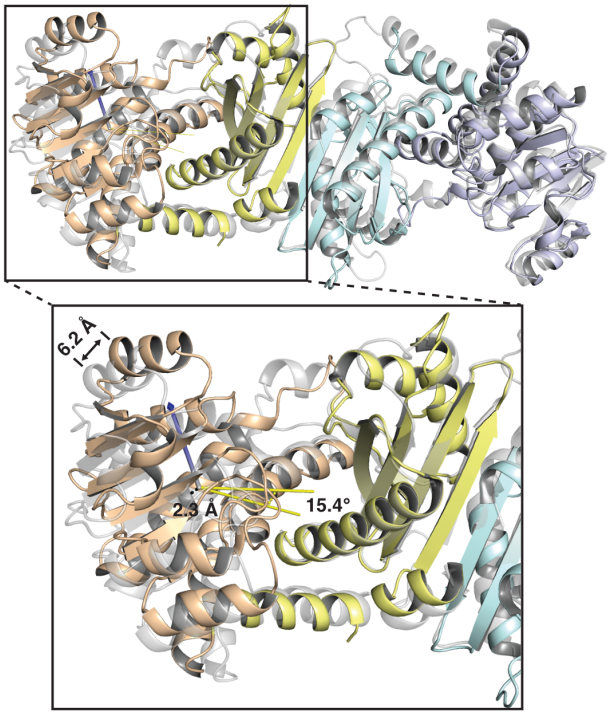

Fig. 4. Comparison of the subunit with the homolog. The domain I of *Pa*-LDH is aligned with the domain I (gray) of the *Lsp*-LDH (PDB ID: 1LEH). The displacement of the domain II between two homologs are illustrated using a vector (purple), and the angle and the distance are shown.

1LEH) using domain I using PyMOL (Fig. 4). The angle and the distance between two domain II were 15.4° and 2.3 Å calculated by the plugin of PyMOL (Angle-between-domains ©2010-2012 Thomas Holder, Max Planck Institute for Developmental Biology). In addition, the farthest helix (H7) from the dimeric interface is moved 6.2 Å toward domain II. Thus, the subunit of *Pa*-LDH is more compact and has a narrower channel for the substrate than the other homologs. We also examined the crystal structure of *Pa*-LDH combined with the multiple sequence alignments to identify the factors affecting thermostability. Three unique intramolecular interactions utilizing non-conserved arginine residues (Arg-270, Arg-293, and Arg-306) observed in the crystal structure could contribute to its stability (Fig. 5, Supplementary Fig. S1). The Arg-270 residue at the end of H10 forms an H-bond with the carbonyl oxygen of Leu-245 in the loop located between H9 and S11 (Fig. 5A). The distance of the H-bond is 2.9 Å. The counterpart residue of the Arg-270 is leucine or methionine in the homolog. The Arg-306 forms a salt bridge with Glu-313, which makes a slightly bent α-helix (Fig. 5B). The other salt bridge is formed by Glu-73 and Arg-293 (Fig. 5B). Two domains of the LDH are tied via a salt bridge between Glu-73 and Arg-293. In addition, the mutation of the triple arginine residues to glutamate residues was shown a reduced enzyme activity to one third, which further reflected those three arginine residues play a key role in the stability (Fig. 5C).

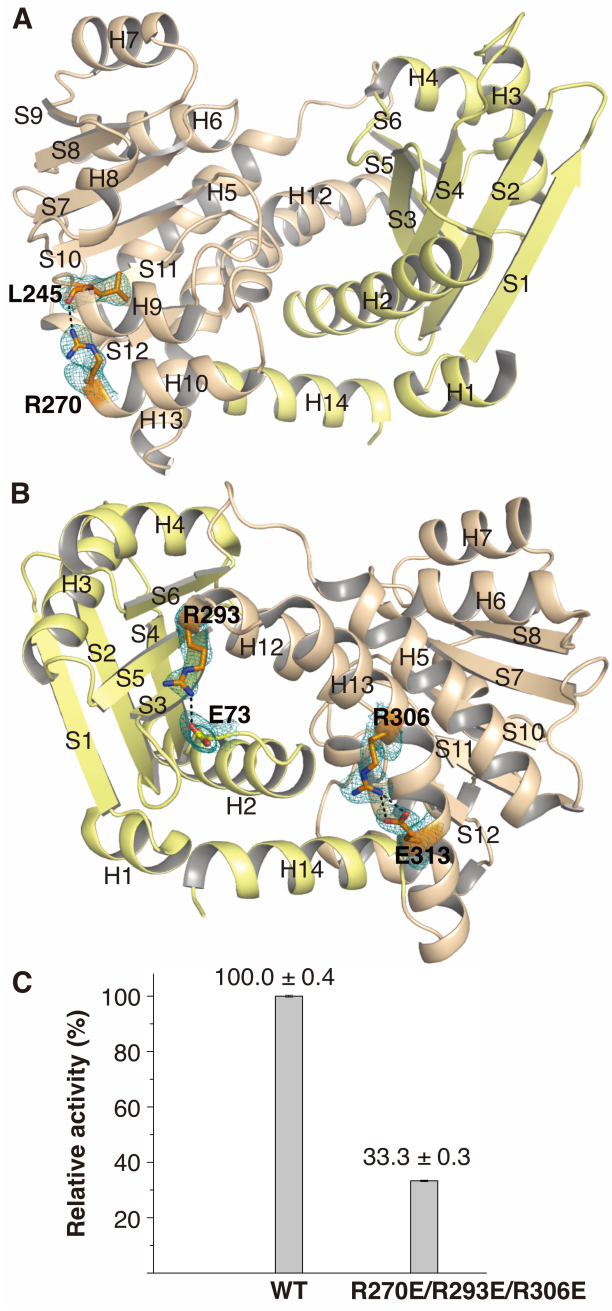

Fig. 5. Overall fold of the monomeric *Pa*-LDH structure. The stick models for the H-bond and salt bridge are shown. The dashed line represents the H-bond and the salt bridge. The *2Fo-Fc* electron density maps for the stick models were contoured at 1.0 σ. (A) Same view as Fig. 1. (B) Backside view of Fig. 1. (C) Mean relative specific activities of the wild type (WT) and mutant (R270E/R293E/R306E) at 37°C and pH 8.5. The specific activity of the WT was set to 100%. Data represent the mean ± SE from three independent measurements.

Enzyme kinetics

We initially determined the mean relative specific activities

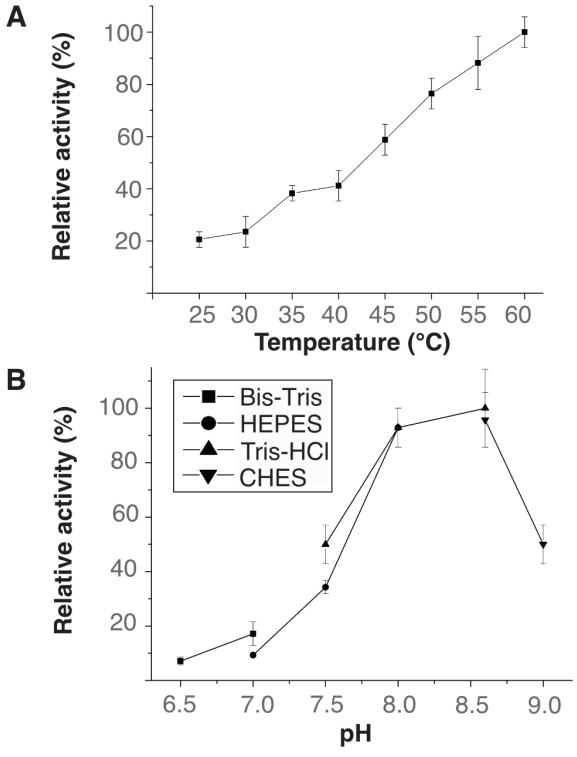

Fig. 6. Mean relative specific activities of *Pa*-LDH at various temperatures and pH levels. The specific activity at 60°C and pH 8.5 was set to 100%. Data represent the mean ± SE from three independent measurements. The reaction conditions were the same except for (A) the temperature, or (B) pH and the buffer component.

at the various temperature and pH level. Since T_m was determined as 61.1°C (Fig. 2C), the enzyme assay was performed from 25°C to 60°C. The mean relative specific activity showed a linear increase in the given temperature range, with the maximum value was achieved at 60°C (Fig. 6A). To determine the optimum pH, we prepared four types of buffers in the pH range (6.5-9.0) using Bis-Tris (pK_a = 6.46), HEPES (pK_a = 7.3), Tris-HCl (pK_a = 8.1), and CHES (pK_a = 9.3). The mean relative specific activity was maximum at pH 8.6 using Tris-HCl buffer (Fig. 6B). We also performed Michaelis-Menten kinetic analysis at 37°C to determine the kinetic parameters for three amino acids, leucine, isoleucine, and valine, and the cofactor, NAD^+ (Table 1, Supplementary Fig. S4). The K_m value for leucine, isoleucine, valine, and NAD^+ were determined to be 1.1, 0.4, 0.5, and 0.2, respectively. Interestingly, *Pa*-LDH was more active with the valine than the other amino acids, as the turnover number (k_{cat}) and specificity constant (k_{cat} / K_m) of the valine were higher than leucine. On the contrary, *Lsp*-LDH was more active with the leucine than the others including the valine (Ohshima et al., 1978).

NAD^+-binding site

To depict the binding pocket for the NAD^+, the crystal structure of this study was superimposed on the structure of the NAD^+-bound *Gst*-LDH (PDB ID: 6ACH) (Fig. 7). Structural comparison indicates that the crystal structure of *Pa*-LDH adopts an open conformation, and the active site residues involved in binding NAD^+ are highly conserved between the two species (Figs. 7A and 7B). The Arg-202 residue, however, is a unique residue in *P. aeruginosa*, as its counterpart amino acid in the other homolog is the alanine or valine (Supplementary Fig. S1). Recently, the mutational study of

Table 1. Kinetic parameters for three different amino acids and the cofactor

Substrate	K_m (mM)	V_{max} (μM s^{-1} mg $protein^{-1}$)	k_{cat} (s^{-1})	k_{cat}/K_m (s^{-1} mM^{-1})
Leucine	1.1 ± 0.1	351.0 ± 18.6	5.2 ± 0.5	4.3 ± 0.7
Isoleucine	0.4 ± 0.1	131.2 ± 4.5	1.8 ± 0.1	5.8 ± 0.4
Valine	0.5 ± 0.1	583.6 ± 18.8	9.6 ± 0.8	14.4 ± 0.9
NAD^+	0.2 ± 0.1	387.3 ± 31.9	3.2 ± 0.03	47.9 ± 1.2

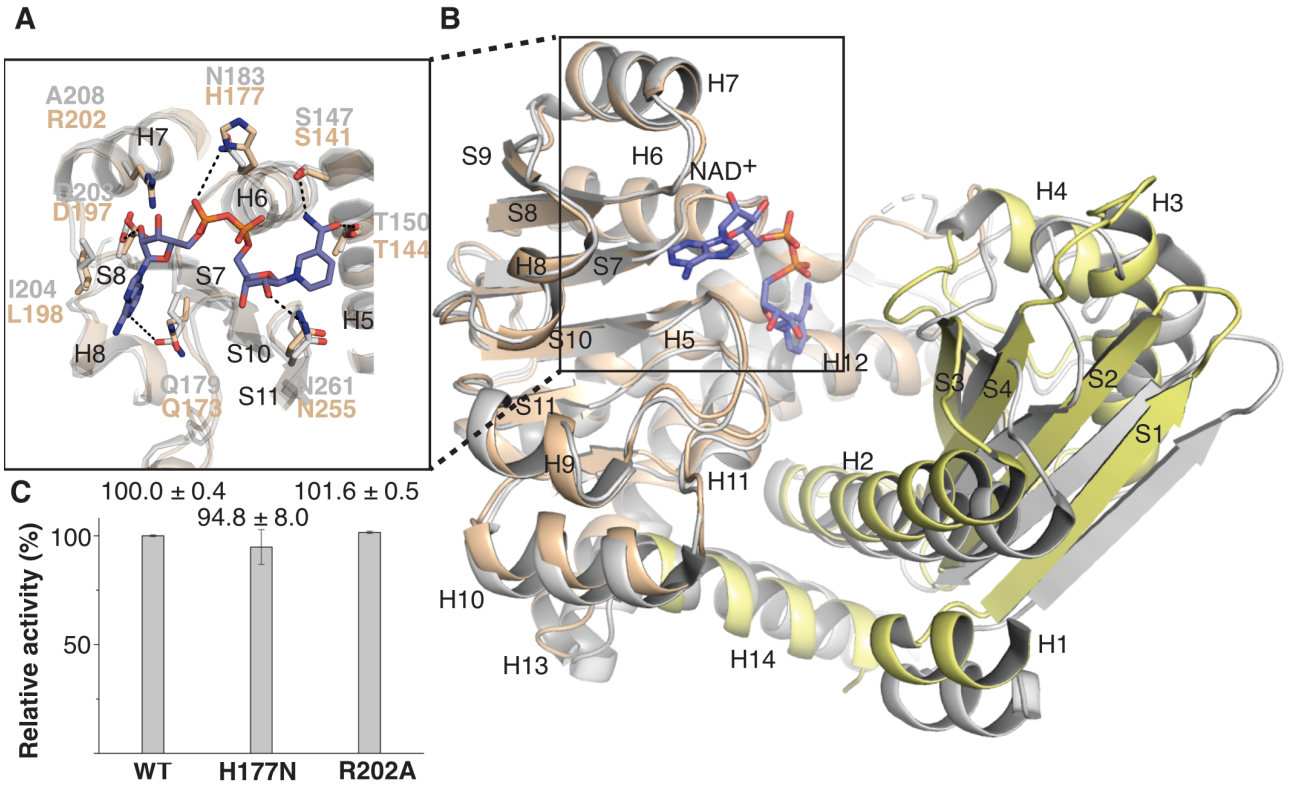

Fig. 7. Structural alignment of domain II in *Pa*-LDH with the crystal structure of domain II in *Gst*-LDH complexed with NAD^+ (PDB ID: 6ACH). (A) Structural alignment of domain II in *Pa*-LDH with domain II in *Gst*-LDH bound to NAD^+ (C atoms in purple, O atoms in red, N atoms in blue, P atoms in orange). (B) Structural alignment of the active site residues in *Pa*-LDH with the active site residues of *Gst*-LDH bound to NAD^+. (C) Mean relative specific activities of the wild type (WT) and mutants (H177N and R202A) at 37°C and pH 8.5. The specific activity of the WT was set to 100%. Data represent the mean ± SE from three independent measurements.

H177N was shown that it has improved catalytic activity for trimethylpyruvate (TMP) (Meng et al., 2021). In our study, the enzyme activity of two mutants, H177N and R202A, from *P. aeruginosa* is indistinguishable from the wild type (Fig. 7C).

In conclusion, we determined the crystal structure of *Pa*-LDH at 2.5 Å resolution. Notably, *Pa*-LDH exists as a dimer in the crystal lattice, as well as in solution. The difference of the quaternary structure is associated with the absence of a tail at the C-terminus. Although the quaternary structure is quite different with the LDH from mesophiles, the thermostability is similar. The key features for the thermostability can be deduced from our crystal structure. Although the dimeric interface is conserved in the homolog, the angles between domain I and domain II are narrow in *Pa*-LDH. Furthermore, three unique arginine residues in *Pa*-LDH makes more compact subunit which makes more stable enzyme. The mutations of three arginine residues to the counterpart charged-amino acid, i.e., glutamate, reduced the enzyme activity to one third of the wild type. The kinetic parameters for the substrates (leucine, isoleucine, and valine), and the cofactor (NAD^+) were determined (Table 1). Surprisingly, *Pa*-LDH was more specific and active on the valine than the leucine. As an important enzyme in pharmaceutical industry, our study will expand our knowledge on the biochemistry of amino acid metabolism and lay the groundwork for its future studies.

Note: Supplementary information is available on the Molecules and Cells website (www.molcells.org).

ACKNOWLEDGMENTS

This research was supported by the Basic Science Research Program of the National Research Foundation of Korea (grant No. 2019R1F1A1063268 to J.K.Y., grant No. 2022R1C1C1004221 to W.K., and grant No. 2021R1A6A1A10044154 to W.K.). We would like to thank the staff at the 11C beamline at Pohang Accelerator Laboratory for support during data collection and the staff at the Korea Basic Science Institute (KBSI) for SEC-MALS and CD measurements.

AUTHOR CONTRIBUTIONS

S.K. (Seheon Kim) and S.K.(Seri Koh) performed experiments. S.K. (Seheon Kim), W.K., and J.K.Y. analyzed the data, and wrote the manuscript.

CONFLICT OF INTEREST

The authors have no potential conflicts of interest to disclose.

ORCID

Seheon Kim https://orcid.org/0000-0002-9582-5253
Seri Koh https://orcid.org/0000-0001-9079-661X
Wonchull Kang https://orcid.org/0000-0001-6517-3533
Jin Kuk Yang https://orcid.org/0000-0003-3824-9963

REFERENCES

Abrahamson, M.J., Vazquez-Figueroa, E., Woodall, N.B., Moore, J.C., and Bommarius, A.S. (2012). Development of an amine dehydrogenase for synthesis of chiral amines. Angew. Chem. Int. Ed. Engl. *51*, 3969-3972.

Baker, P.J., Turnbull, A.P., Sedelnikova, S.E., Stillman, T.J., and Rice, D.W. (1995). A role for quaternary structure in the substrate specificity of leucine dehydrogenase. Structure *3*, 693-705.

Beckett, P.R., Hardin, D.S., Davis, T.A., Nguyen, H.V., Wray-Cahen, D., and Copeland, K.C. (1996). Spectrophometric assay for measuring branched-chain amino acid concentrations: application for measuring the sensitivity of protein metabolism to insulin. Anal. Biochem. *240*, 48-53.

Emsley, P., Lohkamp, B., Scott, W.G., and Cowtan, K. (2010). Features and development of Coot. Acta Crystallogr. D Biol. Crystallogr. *66*, 486-501.

Gasteiger, E., Hoogland, C., Gattiker, A., Duvaud, S., Wilkins, M.R., Appel, R.D., and Bairoch, A. (2005). Protein identification and analysis tools on the ExPASy server. In The Proteomics Protocols Handbook, J.M. Walker, eds. (Totowa, USA: Humana Press), pp. 571-607.

Gu, K.F. and Chang, T.M. (1990a). Conversion of ammonia or urea into essential amino acids, L-leucine, L-valine, and L-isoleucine, using artificial cells containing an immobilized multienzyme system and dextran-NAD+. 2. Yeast alcohol dehydrogenase for coenzyme recycling. Biotechnol. Appl. Biochem. *12*, 227-236.

Gu, K.F. and Chang, T.M. (1990b). Production of essential L-branched-chain amino acids in bioreactors containing artificial cells immobilized multienzyme systems and dextran-NAD+. Biotechnol. Bioeng. *36*, 263-269.

Liebschner, D., Afonine, P.V., Baker, M.L., Bunkoczi, G., Chen, V.B., Croll, T.I., Hintze, B., Hung, L.W., Jain, S., McCoy, A.J., et al. (2019). Macromolecular structure determination using X-rays, neutrons and electrons: recent developments in Phenix. Acta Crystallogr. D Struct. Biol. *75*, 861-877.

Meng, X., Yang, L., Liu, Y., Wang, H., Shen, Y., and Wei, D. (2021). Identification and rational engineering of a high substrate-tolerant leucine dehydrogenase effective for the synthesis of L-tert-leucine. ChemCatChem *13*, 3340-3349.

Ohshima, T., Misono, H., and Soda, K. (1978). Properties of crystalline leucine dehydrogenase from Bacillus sphaericus. J. Biol. Chem. *253*, 5719-5725.

Ohshima, T., Nagata, S., and Soda, K. (1985). Purification and characterization of thermostable leucine dehydrogenase from Bacillus stearothermophilus. Arch. Microbiol. *141*, 407-411.

Suzuki, K., Suzuki, K., Koizumi, K., Ichimura, H., Oka, S., Takada, H., and Kuwayama, H. (2008). Measurement of serum branched-chain amino acids to tyrosine ratio level is useful in a prediction of a change of serum albumin level in chronic liver disease. Hepatol. Res. *38*, 267-272.

Tajiri, K. and Shimizu, Y. (2013). Branched-chain amino acids in liver diseases. World J. Gastroenterol. *19*, 7620-7629.

Turnbull, A.P., Ashford, S.R., Baker, P.J., Rice, D.W., Rodgers, F.H., Stillman, T.J., and Hanson, R.L. (1994). Crystallization and quaternary structure analysis of the NAD(+)-dependent leucine dehydrogenase from Bacillus sphaericus. J. Mol. Biol. *236*, 663-665.

Winn, M.D., Ballard, C.C., Cowtan, K.D., Dodson, E.J., Emsley, P., Evans, P.R., Keegan, R.M., Krissinel, E.B., Leslie, A.G., McCoy, A., et al. (2011). Overview of the CCP4 suite and current developments. Acta Crystallogr. D Biol. Crystallogr. *67*, 235-242.

Yamaguchi, H., Kamegawa, A., Nakata, K., Kashiwagi, T., Fujiyoshi, Y., Tani, K., and Mizukoshi, T. (2021). Leucine dehydrogenase: structure and thermostability. Subcell. Biochem. *96*, 355-372.

Yamaguchi, H., Kamegawa, A., Nakata, K., Kashiwagi, T., Mizukoshi, T., Fujiyoshi, Y., and Tani, K. (2019). Structural insights into thermostabilization of leucine dehydrogenase from its atomic structure by cryo-electron microscopy. J. Struct. Biol. *205*, 11-21.

Zhao, Y., Wakamatsu, T., Doi, K., Sakuraba, H., and Ohshima, T. (2012). A psychrophilic leucine dehydrogenase from Sporosarcina psychrophila: purification, characterization, gene sequencing and crystal structure analysis. J. Mol. Catal. B Enzym. *83*, 65-72.